

First Direct Observation of Collider Neutrinos with FASER at the LHC

Henso Abreu¹, John Anders², Claire Antel³, Akitaka Ariga^{4,5}, Tomoko Ariga⁶, Jeremy Atkinson⁴, Florian U. Bernlochner⁷, Tobias Blesgen⁷, Tobias Boeckh⁷, Jamie Boyd², Lydia Brenner⁸, Franck Cadoux³, David W. Casper⁹, Charlotte Cavanagh¹⁰, Xin Chen¹¹, Andrea Coccaro¹², Ansh Desai¹³, Sergey Dmitrievsky¹⁴, Monica D'Onofrio¹⁰, Yannick Favre³, Deion Fellers¹³, Jonathan L. Feng⁹, Carlo Alberto Fenoglio³, Didier Ferrere³, Stephen Gibson¹⁵, Sergio Gonzalez-Sevilla³, Yuri Gornushkin¹⁴, Carl Gwilliam¹⁰, Daiki Hayakawa⁵, Shih-Chieh Hsu¹⁶, Zhen Hu¹¹, Giuseppe Iacobucci³, Tomohiro Inada¹¹, Sune Jakobsen², Hans Joos^{2,17}, Enrique Kajomovitz¹, Hiroaki Kawahara⁶, Alex Keyken¹⁵, Felix Kling¹⁸, Daniela Köck¹³, Umut Kose², Raffaella Kotitsa², Susanne Kuehn², Helena Lefebvre¹⁵, Lorne Levinson¹⁹, Ke Li¹⁶, Jinfeng Liu¹¹, Jack MacDonald²⁰, Chiara Magliocca³, Fulvio Martinelli³, Josh McFayden²¹, Matteo Milanese³, Dimitar Mladenov², Théo Moretti³, Magdalena Munker³, Mitsuhiro Nakamura²², Toshiyuki Nakano²², Marzio Nessi^{3,2}, Friedemann Neuhaus²⁰, Laurie Nevay^{2,15}, Hidetoshi Otono⁶, Hao Pang¹¹, Lorenzo Paolozzi^{3,2}, Brian Petersen², Francesco Pietropaolo², Markus Prim⁷, Michaela Queitsch-Maitland²³, Filippo Resnati², Hiroki Rokujo²², Elisa Ruiz-Choliz²⁰, Jorge Sabater-Iglesias³, Osamu Sato²², Paola Scampoli^{4,24}, Kristof Schmieden²⁰, Matthias Schott²⁰, Anna Sfyrila³, Savannah Shively⁹, Yosuke Takubo²⁵, Noshin Tarannum³, Ondrej Theiner³, Eric Torrence¹³, Serhan Tufanli², Svetlana Vasina¹⁴, Benedikt Vormwald², Di Wang¹¹, Eli Welch⁹, and Stefano Zambito³

(FASER Collaboration)

¹Department of Physics and Astronomy, Technion—Israel Institute of Technology, Haifa 32000, Israel

²CERN, CH-1211 Geneva 23, Switzerland

³Département de Physique Nucléaire et Corpusculaire, University of Geneva, CH-1211 Geneva 4, Switzerland

⁴Albert Einstein Center for Fundamental Physics, Laboratory for High Energy Physics, University of Bern, Sidlerstrasse 5, CH-3012 Bern, Switzerland

⁵Department of Physics, Chiba University, 1-33 Yayoi-cho Inage-ku, 263-8522 Chiba, Japan

⁶Kyushu University, Nishi-ku, 819-0395 Fukuoka, Japan

⁷Universität Bonn, Regina-Pacis-Weg 3, D-53113 Bonn, Germany

⁸Nikhef National Institute for Subatomic Physics, Science Park 105, 1098 XG Amsterdam, Netherlands

⁹Department of Physics and Astronomy, University of California, Irvine, California 92697-4575, USA

¹⁰University of Liverpool, Liverpool L69 3BX, United Kingdom

¹¹Department of Physics, Tsinghua University, Beijing, China

¹²INFN Sezione di Genova, Via Dodecaneso, 33-16146, Genova, Italy

¹³University of Oregon, Eugene, Oregon 97403, USA

¹⁴Affiliated with an international laboratory covered by a cooperation agreement with CERN

¹⁵Royal Holloway, University of London, Egham TW20 0EX, United Kingdom

¹⁶Department of Physics, University of Washington, PO Box 351560, Seattle, Washington 98195-1460, USA

¹⁷II. Physikalisches Institut, Universität Göttingen, Göttingen, Germany

¹⁸Deutsches Elektronen-Synchrotron DESY, Notkestr. 85, 22607 Hamburg, Germany

¹⁹Department of Particle Physics and Astrophysics, Weizmann Institute of Science, Rehovot 76100, Israel

²⁰Institut für Physik, Universität Mainz, Mainz, Germany

²¹Department of Physics and Astronomy, University of Sussex, Sussex House, Falmer, Brighton BN1 9RH, United Kingdom

²²Nagoya University, Furo-cho, Chikusa-ku, Nagoya 464-8602, Japan

²³University of Manchester, School of Physics and Astronomy, Schuster Building, Oxford Rd, Manchester M13 9PL, United Kingdom

²⁴Dipartimento di Fisica “Ettore Pancini”, Università di Napoli Federico II, Complesso Universitario di Monte S. Angelo, I-80126 Napoli, Italy

²⁵Institute of Particle and Nuclear Studies, KEK, Oho 1-1, Tsukuba, Ibaraki 305-0801, Japan



(Received 24 March 2023; accepted 8 May 2023; published 19 July 2023)

We report the first direct observation of neutrino interactions at a particle collider experiment. Neutrino candidate events are identified in a 13.6 TeV center-of-mass energy pp collision dataset of 35.4 fb^{-1} using the active electronic components of the FASER detector at the Large Hadron Collider. The candidates are

required to have a track propagating through the entire length of the FASER detector and be consistent with a muon neutrino charged-current interaction. We infer 153_{-13}^{+12} neutrino interactions with a significance of 16 standard deviations above the background-only hypothesis. These events are consistent with the characteristics expected from neutrino interactions in terms of secondary particle production and spatial distribution, and they imply the observation of both neutrinos and anti-neutrinos with an incident neutrino energy of significantly above 200 GeV.

DOI: [10.1103/PhysRevLett.131.031801](https://doi.org/10.1103/PhysRevLett.131.031801)

Introduction.—Since their discovery at a nuclear reactor in 1956 [1], neutrinos have been detected from a variety of sources: fixed target experiments [2], cosmic ray interactions in the atmosphere [3–5], the Sun [6,7], the Earth [8], supernovae [9,10], and astrophysical bodies outside our galaxy [11]. With each new source has come new insights, with important implications for many fields, from particle physics to geophysics to astrophysics and cosmology.

Until now, however, no neutrino produced at a particle collider has ever been directly detected. Colliders copiously produce both neutrinos and antineutrinos of all flavors, and they do so in a range of very high energies where neutrino interactions have not yet been observed. Nevertheless, collider neutrinos have escaped detection, because they interact extremely weakly, and the highest energy neutrinos, which have the largest probability of interacting, are dominantly produced in the forward region, parallel to the beamline [12–18], where collider detectors typically have uninstrumented regions to allow the entry and exit of the colliding particle beams. In 2021, the FASER Collaboration identified the first collider neutrino candidates [19] using a 29 kg pilot detector, highlighting the potential of discovering collider neutrinos in the forward region of the Large Hadron Collider (LHC) collisions. In addition to FASER, the SND@LHC experiment is expected to observe and study neutrinos produced in the LHC collisions [20–22] and recently reported preliminary findings [23]. The observation of collider neutrino interactions will have wide ranging implications for the study of neutrino properties, QCD, astroparticle physics, and searches for physics beyond the standard model [24].

This Letter reports the first direct observation of neutrinos produced at a particle collider by analyzing 35.4 fb^{-1} of proton-proton (pp) collision data from run 3 of the LHC at a center-of-mass energy of 13.6 TeV. Neutrinos of all flavors are produced in the decays of light and heavy hadrons as a high-intensity beam along the collision axis. In this Letter we focus on the charged-current (CC) interactions of ν_μ and $\bar{\nu}_\mu$; in the following, charge conjugation

and natural units are implied throughout. The chosen analysis strategy is designed to be independent of the simulation of the detector response and therefore does not measure the neutrino interaction cross section, but rather the significance of the observed number of neutrino candidate events over the non-neutrino background. In addition to being the first collider neutrinos ever observed, the neutrinos detected here are expected to be the most energetic ever detected from a human source, with energies in the unexplored range 360 GeV–6.3 TeV between fixed target measurements [25] and astroparticle data [26].

The FASER detector.—FASER [17,27–29], the ForwArd Search ExpeRiment, is an apparatus dedicated to searching for light, extremely weakly interacting particles and studying neutrinos. A detailed description can be found in Ref. [27]. The experiment is located in the TI12 tunnel, which connects the Super Proton Synchrotron (SPS) and LHC tunnels, approximately 480 m downstream of the ATLAS interaction point (IP) and aligned with the collision axis line of sight (LOS). Charged particles produced in the forward direction at the ATLAS IP are deflected by LHC magnets, and FASER is also shielded from the ATLAS IP by about 100 m of rock and concrete. FASER’s location therefore ensures that a high-intensity beam of neutrinos traverses the detector, while backgrounds are highly suppressed.

The FASER detector is partially immersed in a magnetic field and consists of a passive tungsten-emulsion neutrino detector (FASER ν), two scintillator-based veto systems, additional scintillators for triggering, a tracking spectrometer, a preshower scintillator station, and an electromagnetic calorimeter. For the current analysis, the most important components are the veto systems, the tracking spectrometer, and the tungsten target of the FASER ν detector. A schematic of the FASER detector is depicted in Fig. 1. The trigger and data acquisition system of FASER was designed to achieve high efficiency and reliability [30]. Neutrino candidate events are triggered by scintillator signals that exceed a preset threshold below that of a single minimum-ionizing particle (MIP), resulting in a typical trigger rate of 0.5–1.3 kHz.

FASER ν consists of 730 layers of 1.1 mm-thick tungsten plates interleaved with emulsion films. With a width of 25 cm and a height of 30 cm, it has a total mass of 1.1 metric tons. Although the emulsion films provide excellent

Published by the American Physical Society under the terms of the [Creative Commons Attribution 4.0 International license](https://creativecommons.org/licenses/by/4.0/). Further distribution of this work must maintain attribution to the author(s) and the published article’s title, journal citation, and DOI. Funded by SCOAP³.

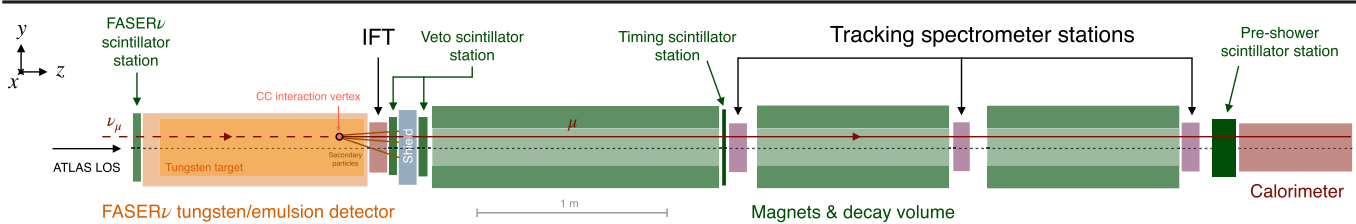


FIG. 1. Schematic side view of the FASER detector with a muon neutrino undergoing a CC interaction in the emulsion-tungsten target.

position and angular resolution to identify CC neutrino interactions, they are not used as the extraction, scanning and analysis is time intensive. Instead, the FASER ν detector is used as a target for CC neutrino interactions, and we rely on the active electronic detector components of FASER to identify suitable muon neutrino candidates [31].

The FASER scintillator stations are instrumental to identify suitable neutrino candidates and veto charged particles originating from the interaction point or from secondary interactions. The first veto system (FASER ν scintillator station) is located in front of the FASER ν emulsion detector. It is constructed from two modules of $30\text{ cm} \times 35\text{ cm}$, 2 cm-thick plastic scintillators, which are read out with photomultiplier tubes (PMTs). The second veto system (veto scintillator station) is located after the FASER ν emulsion detector and in front of the first magnet. It is built from three planes of the same plastic scintillators, arranged with a 10 cm-thick lead block placed between the first and second planes. The lead acts as an additional target for neutrino interactions and to absorb or convert high-energy photons from muon bremsstrahlung.

The tracking system consists of the interface tracking station (IFT) and the three tracking spectrometer stations [32]. Each tracking station is composed of three planes with eight ATLAS semiconductor tracker (SCT) barrel modules [33] per plane, arranged as two columns of four modules. Each SCT module consists of a double-layer of single-sided silicon microstrips with a 40 mrad stereo angle and an $80\text{ }\mu\text{m}$ strip pitch. To identify muons from CC interactions, only the tracking spectrometer stations are used, whereas the IFT's location after the tungsten-emulsion detector makes it ideal to study remnants and secondary particles of CC deep inelastic scattering neutrino interactions. A muon candidate traversing the full length of the spectrometer produces 18 silicon hits. Adjacent silicon hits in the tracking stations are combined into clusters. Between the three tracking spectrometer stations are two 1 m-long dipole magnets with magnetic field of 0.57 T, with a similar 1.5 m-long magnet in front of the spectrometer. The magnets have an aperture of 200 mm diameter, which defines the active transverse area of the detector, and bend charged particles in the vertical plane. In addition, signals from the timing scintillator station, located between the first and second magnet and in front of the first tracking station of the spectrometer, are used. The scintillator

stations in combination with the tracking system are capable of reliably identifying incoming charged particles passing through the full length of FASER with inefficiencies smaller than 10^{-7} , depending on the momentum and other requirements in the selection.

Dataset and simulated samples.—For this analysis we use data from runs with stable beam conditions collected between July and November 2022, corresponding to a total luminosity of $(35.4 \pm 0.8)\text{ fb}^{-1}$ [34,35] after data quality selection. A detailed description of the analysis is following; additional details are contained in Appendices A–E.

To study the detector response to neutrino interactions, we simulate 4.3×10^4 neutrino events corresponding to an integrated luminosity of approximately 600 fb^{-1} . The interaction with the tungsten-emulsion detector is simulated using the GENIE event generator [36,37]. The neutrino energy spectra and relative flavor composition are based on Ref. [38]. To estimate the number of expected neutrino events, we adjust several of the assumptions of Ref. [38]: we correct the center-of-mass energy, beam crossing angle, and LOS alignment, and we use the average of the neutrino flux from the predicted light and heavy hadron production of DPMJET [39,40] and SIBYLL [41]. The difference between the two individual predictions and the average is 27% and is assigned as an uncertainty. All interactions of particles traversing the FASER detector are simulated using GEANT4 [42].

The main background to neutrino signatures originates from high-momentum muons. We use the energy and angular spectrum predicted by the FLUKA generator [43,44], which includes a detailed description of the LHC machine elements and infrastructure, to simulate a sample of 2×10^6 muons for background studies. Two additional sources of backgrounds are relevant: neutral hadrons produced by muon interactions in the concrete in front of the FASER detector and geometric backgrounds from charged particles missing the FASER ν scintillator.

We use simulated samples to study the neutral hadron backgrounds. The contamination from geometric background events is studied using sidebands and extrapolated into the signal region using simulations. The backgrounds from cosmic rays and LHC beam background have been studied using events occurring when there are no collisions, and are found to be negligible.

Selection and background rejection.—We focus on identifying ν_μ and $\bar{\nu}_\mu$ CC interactions produced in the

tungsten-emulsion detector. Such interactions will produce a high-momentum μ that can be reconstructed in the three stations of the FASER tracking spectrometer. In addition, we expect increased activity in the veto and timing scintillator stations and in the IFT tracking station from secondary particles produced in the CC interaction. To avoid unconscious bias, a blind analysis was carried out where the event selection, background estimations, and systematic uncertainties were fixed prior to looking at data in the signal-enhanced region.

We select events triggered by any of the scintillators downstream of FASER ν . To discard signals from beam backgrounds and cosmic muons, we further require a timing stamp consistent with a colliding bunch crossing identifier. We use the FASER ν scintillator to identify backgrounds from muons or other charged particles entering the FASER detector and reject events that deposit a charge of more than 40 pC in the PMTs. Such a charge deposition would be consistent with the presence of one or several MIPs. We only look for CC interactions that produce a muon that traverses the entire length of the FASER detector. The signals in the scintillators downstream of the lead wall in the veto system, and in the calorimeter, are therefore required to be compatible with those of a MIP. With the three tracker stations we reconstruct events with exactly one track and require more than 11 silicon hits in the tracking stations. The reconstructed tracks are required to have a reasonable track fit quality, and we require the reconstructed track momentum to fulfill $p_\mu > 100$ GeV. To reject charged particles, whose trajectory geometrically missed the FASER ν scintillator station, we extrapolate the reconstructed track from the spectrometer back to the IFT and FASER ν scintillator. The track's extrapolation to the IFT must lie within 95 mm of the detector's central axis, and its extrapolation to the FASER ν scintillator must be at a distance of $r_{\text{veto } \nu} < 120$ mm from the FASER ν scintillator center.

Neutral hadron and geometric backgrounds.—To estimate the number of neutral hadrons that reach FASER, we simulate 2.1×10^9 μ events based on the FLUKA energy spectrum, and use GEANT4 to propagate through the last 8 m of rock in front of FASER. From this sample we determine the number of neutral hadrons with a momentum larger than 100 GeV that reach the detector. The selection efficiency is evaluated with an additional sample of neutral kaons and neutrons with momenta larger than 100 GeV in front of the FASER ν emulsion detector. Most simulated hadrons are absorbed in the tungsten or do not produce a charged track with sufficient momentum to pass the signal selection and only a small fraction of the simulated hadrons pass all selection steps. From this we estimate the total neutral hadron background to be $n_{\text{had}} = 0.11 \pm 0.06$, with the uncertainty denoting the statistical error. Further simulation studies show that in most cases the parent muon

enters the detector along with the neutral hadron. Such events would be rejected by the FASER ν veto scintillator. The estimate assumes that all neutral hadron events are not already vetoed by the accompanying muon, and is therefore a conservative estimate of this background contribution.

To estimate the geometric background contribution, we count the number of background events n_{geo} using a sideband and apply a scaling to the signal region of f_{geo} , which is extracted from simulated samples. The sideband is defined to enhance the contribution of muons that miss the FASER ν scintillator station, but may be able to produce a track in the spectrometer, which passes the selection by scattering in the tungsten and/or bending in the magnetic field. We modify the event selection outlined above: we require at most 8 IFT clusters, an extrapolated radius r_{IFT} of 90 to 95 mm with respect to the IFT center, and apply no selection on $r_{\text{veto } \nu}$. None of the selected sideband events have a momentum larger than 100 GeV. We thus extrapolate to the signal region by using a linear fit to the momentum distribution. We correct this estimate to account for the $r_{\text{veto } \nu}$ selection by using the ratio of events with a radius smaller than 120 mm over all sideband events in the fitted range. As we observe no events with $r_{\text{veto } \nu} < 120$ mm in the fitted range, we use the 3σ upper limit of the expectation value of a Poisson process for an observation of zero events of 5.9. With this we find $n_{\text{geo}} = 0.01 \pm 0.23$ background events in the sideband, with the uncertainty denoting the statistical error. We extract a scaling factor between this sideband and the signal region from simulations, probing different momenta, angles, and position ranges, and use the resulting deviation from the nominal simulation scenario as an uncertainty. This results in a scaling factor of $f_{\text{geo}} = 7.9 \pm 2.4$ and a total geometric background estimate of 0.08 ± 1.83 events.

Results.—Figure 2 shows the selected events, as well as the background-enriched regions with lower momentum or $r_{\text{veto } \nu} > 120$ mm. In total we observe 153 events passing all selection steps. Using GENIE we study the composition of neutrino events passing this selection and find that 99% originate from muon neutrino CC interactions.

We group the selected events into four categories to estimate the number of neutrino (n_ν) and background events (n_b). The categorization is determined by whether the events pass or fail the FASER ν veto scintillator selection criteria. This allows us to determine in a simulation-independent way the inefficiencies of the two layers of the FASER ν veto scintillator (p_1, p_2) under the assumption that they are uncorrelated.

Besides the signal category, we select:
 n_{10} : Events for which the first layer of the FASER ν scintillator produces a charge of >40 pC in the PMT, but no signal with sufficient charge is seen in the second layer.

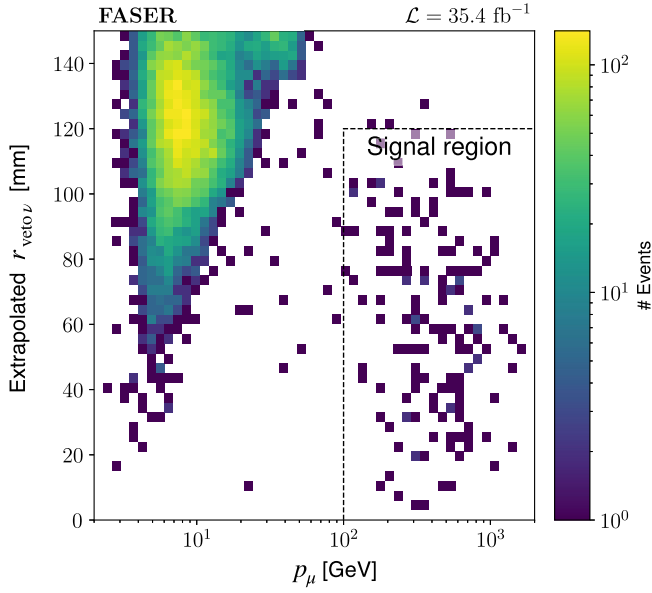


FIG. 2. The selected signal region in extrapolated radius $r_{\text{veto}\nu}$ and reconstructed track momentum p_{μ} is depicted. The region with lower momenta and larger radii is dominated by background events consisting of charged particles that miss the FASER ν scintillator station.

n_{01} : Analogous events for which more than 40 pC in the PMT was observed in the second layer, but not in the first layer.

n_2 : Events for which both layers observe more than 40 pC of charge.

Table I lists the observed event yields and their relation to the expected number of neutrino and background events and the FASER ν veto scintillator inefficiencies.

We analyze the observed number of events using a binned extended maximum likelihood fit, implemented using the `iminuit` package [45]. We introduce nuisance parameters to constrain the estimated background events to their expectations using Gaussian priors. The likelihood is numerically maximized, and we use a discovery test statistic [46] to determine the significance of the observed signal over the background-only hypothesis. We find

$$n_{\nu} = 153_{-13}^{+12}(\text{stat}) \pm 2(\text{bkg}) = 153_{-13}^{+12}(\text{tot})$$

TABLE I. Observed event yields in 35.4 fb $^{-1}$ of collision data and their relation to neutrino and background events.

Category	Events	Expectation
Signal	153	$n_{\nu} + n_b \cdot p_1 \cdot p_2 + n_{\text{had}} + n_{\text{geo}} \cdot f_{\text{geo}}$
n_{10}	4	$n_b \cdot (1 - p_1) \cdot p_2$
n_{01}	6	$n_b \cdot p_1 \cdot (1 - p_2)$
n_2	64 014 695	$n_b \cdot (1 - p_1) \cdot (1 - p_2)$

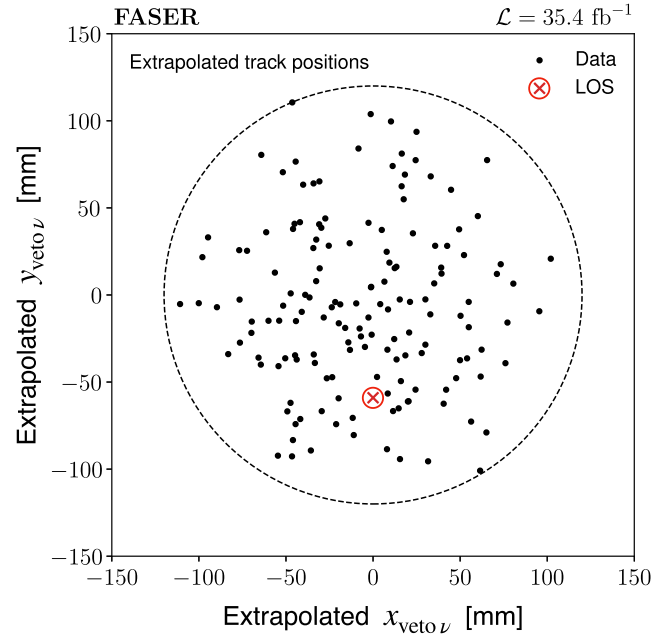


FIG. 3. Extrapolated transverse position of the reconstructed tracks of neutrino-like events to the FASER ν scintillator station. The ATLAS LOS is indicated with a red marker and shifted 59 mm in the negative y direction from the center of the scintillator station.

with a significance of 16 standard deviations over the background-only hypothesis and based on the asymptotic distribution of the test statistic. The excess is compatible with the expected number of neutrino events $n_{\nu}^{\text{exp}} = 151 \pm 41$, but note that its error does not include any systematic uncertainties from simulating the detector response and selection. The determined inefficiencies of the two FASER ν scintillators are $p_1 = (6_{-3}^{+4}) \times 10^{-8}$ and $p_2 = (9_{-3}^{+4}) \times 10^{-8}$, showing values close to the expected performance [27].

We expect that the identified neutrino candidates are distributed around the ATLAS LOS and do not cluster at a specific point of origin. We test this by using the extrapolated position to the FASER ν scintillator station from the reconstructed tracks of the neutrino-like events in the signal category. Figure 3 shows the extrapolated positions and we observe the expected behavior.

Figure 4 summarizes additional properties of the signal category events. The CC neutrino interactions produce on average a larger number of particles than MIP interactions, which appear in the IFT as charge depositions. The number of IFT clusters of the signal category is very distinct from backgroundlike (n_2) events and agrees well with the expectation from GENIE. We also examine the polar angles θ_{μ} of the neutrino candidates and observe distributions close to the simulated neutrino events and distinctively different from muon backgrounds. We observe a clear charge separation in q/p_{μ} for the reconstructed tracks, with

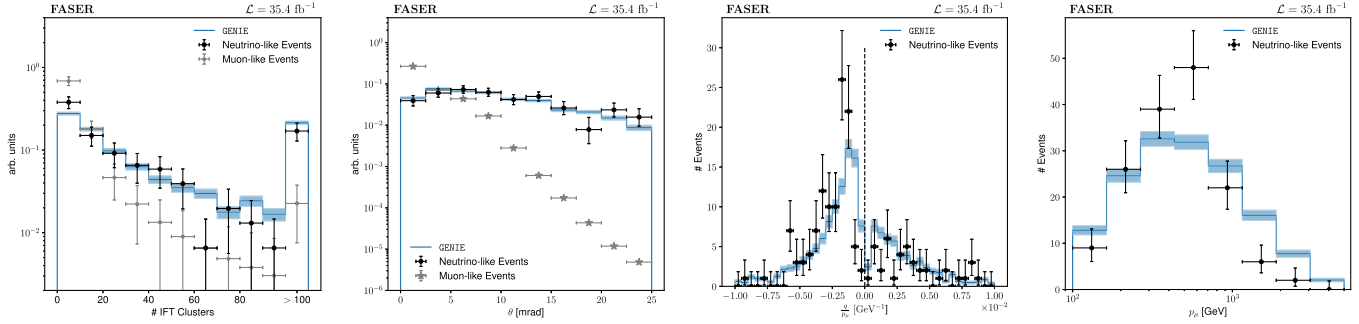


FIG. 4. The figures depict the number of reconstructed clusters in the IFT, track polar angle θ_μ , q/p_μ , and the reconstructed momentum p_μ for events in the signal region (black markers) and compare them to the expectation from GENIE (blue) and muon-like events (gray markers). The muonlike events are from the n_2 category, for which both layers of the FASER ν scintillator observed a signal, and show the expected distributions for non-neutrino backgrounds. The blue bands correspond to the statistical error of the simulated samples and are luminosity scaled for q/p_μ and p_μ . The other figures are normalized to unity.

q denoting the assigned track charge. In total 40 events with a positively charged track candidate are observed, showing the presence of antineutrinos in the analyzed dataset. The reconstructed momentum of the muon produced in a CC ν_μ interaction is a good proxy for the incident neutrino energy. Using the simulated CC neutrino interactions, we estimate that with our analysis strategy we select neutrino events for which on average $> 80\%$ of the incident neutrino momentum is transferred to the final state muon. This indicates that a large fraction of the reconstructed neutrino candidates have energies significantly larger than 200 GeV. A detailed study of these properties, which accounts for systematic effects, is left for future work.

Summary.—We report the first direct detection of neutrinos produced at a collider experiment using the active electronic components of the FASER detector. We observe 153^{+12}_{-13} neutrino events from CC interactions from ν_μ and $\bar{\nu}_\mu$ taking place in the tungsten-emulsion detector of FASER ν . The spatial distribution and properties of the observed signal events are consistent with neutrino interactions, and the chosen analysis strategy does not depend on the quality of the modeling of detector effects in the simulation. For the signal events, the reconstructed charge shows the presence of antineutrinos, and the reconstructed momentum implies that neutrino candidates have energies significantly above 200 GeV. This result marks the beginning of the field of collider neutrino physics, opening up a wealth of new measurements with broad implications across many physics domains [24].

We thank CERN for the very successful operation of the LHC during 2022. We thank the technical and administrative staff members at all FASER institutions for their contributions to the success of the FASER project. We thank the ATLAS Collaboration for providing us with accurate luminosity estimates for the used Run 3 LHC collision data. FASER. gratefully acknowledges the donation of spare ATLAS SCT modules and spare LHCb calorimeter modules, without which the experiment would

not have been possible. We also acknowledge the ATLAS Collaboration software, Athena, on which FASER’s offline software system is based [47] and the ACTS tracking software framework [48]. Finally we thank the CERN STI group for providing detailed FLUKA simulations of the muon fluence along the LOS, which have been used in this analysis. This work was supported in part by Heising-Simons Foundation Grants No. 2018-1135, No. 2019-1179, and No. 2020-1840, Simons Foundation Grant No. 623683, U.S. National Science Foundation Grants No. PHY-2111427, No. PHY-2110929, and No. PHY-2110648, JSPS KAKENHI Grants No. JP19H01909, No. JP20K23373, No. JP20H01919, No. JP20K04004, and No. JP21H00082, BMBF Grant No. 05H20PDR1, No. DFG EXC 2121 Quantum Universe Grant No. 390833306, ERC Consolidator Grant No. 101002690, Royal Society Grant No. URF/R1\201519, UK Science and Technology Funding Councils Grant No. ST/T505870/1, the National Natural Science Foundation of China, Tsinghua University Initiative Scientific Research Program, and the Swiss National Science Foundation.

Appendix A: Geometric sideband.—Figure 5 depicts the sideband used to estimate the geometric backgrounds of the analysis. Background events are required to be consistent with a muon candidate by having ≤ 8 IFT clusters and an extrapolated radius r_{IFT} of 90 to 95 mm with respect to the IFT center. This selection is dominated by geometric background events that do not pass the signal selection steps of the analysis. No events with $p_\mu > 100$ GeV are observed. To estimate the number of events within this momentum range, we linearly extrapolate the events between 30 and 100 GeV and find 0.2 ± 4.1 events, with the error denoting the statistical error. To account for the $r_{\text{veto}\nu}$ requirement of the signal selection, we further apply a requirement of $r_{\text{veto}\nu} < 120$ mm to the sideband events (orange distribution). No events with $p_\mu > 30$ GeV are observed. We thus use 5.9 as the 3σ upper limit and use this to

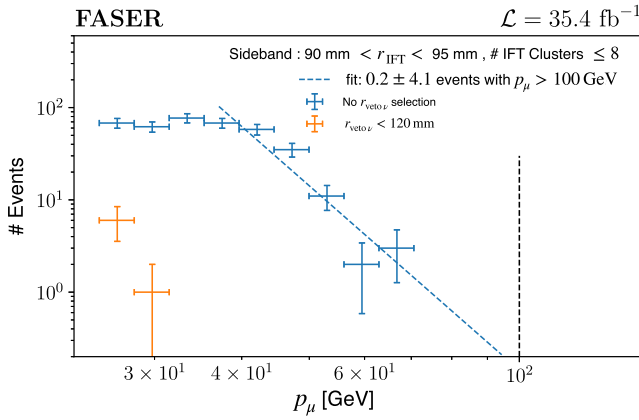


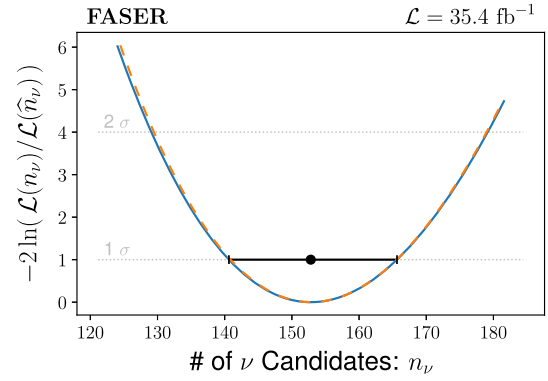
FIG. 5. Sideband for geometric background estimation.

calculate the ratio with respect to the number of events without any r_{vetov} selection, to correct the sideband background events for the r_{vetov} requirement. With this factor we find $n_{\text{geo}} = 0.01 \pm 0.23$ geometric background events. To account for the fact that this number corresponds to an annulus, the correction factor $f_{\text{geo}} = 7.9 \pm 2.4$, determined from simulation, is applied. It is obtained from simulation with the uncertainty spanning different assumptions about the angle, momenta, and positions of the geometric background events.

Appendix B: Event display.—Figure 6 shows an event display of an example neutrino candidate event. The event has a momentum of $p_\mu = 843.9$ GeV, negative charge, $\theta_\mu = 2.5$ mrad, $r_{\text{vetov}} = 57.2$ mm, $r_{\text{IFT}} = 55.8$ mm and produced 57 clusters in the IFT.

Appendix C: Likelihood fit.—The used likelihood has the form

$$\mathcal{L} = \prod_i \mathcal{P}(N_i | n_i) \cdot \prod_j \mathcal{G}_j. \quad (\text{C1})$$


 FIG. 7. The log-likelihood ratio of the estimated number of neutrinos is shown in blue. The dashed orange contour fixes the parameters of \mathcal{G}_i to determine the statistical uncertainty of the neutrino signal yield.

Here \mathcal{P} denotes a Poissonian with the index i running over the four event categories with observed event counts N_i and expectation values n_i . We introduce nuisance parameters to constrain the estimated number of background events to their expectations using three Gaussian priors \mathcal{G}_j . The used test statistic has the form

$$q_0 = \begin{cases} -2 \ln \lambda(n_\nu = 0) & \hat{n}_\nu \geq 0 \\ 0 & \hat{n}_\nu < 0 \end{cases} \quad (\text{C2})$$

and the significance of the observed signal \hat{n}_ν over the background-only hypothesis is given by $\sqrt{q_0}$ in the asymptotic limit. Further $\lambda(n_\nu = 0) := \mathcal{L}(n_\nu = 0) / \mathcal{L}(\hat{n}_\nu)$ denotes the ratio of the likelihood maximized with the condition of no signal, $n_\nu = 0$, to the unconditionally maximized likelihood. The log-likelihood ratio is shown in Fig. 7.

Appendix D: Momentum resolution.—Data-driven alignment corrections are applied to the positions and orientations of the modules of the tracking spectrometer stations using a sample of reconstructed muons. In the

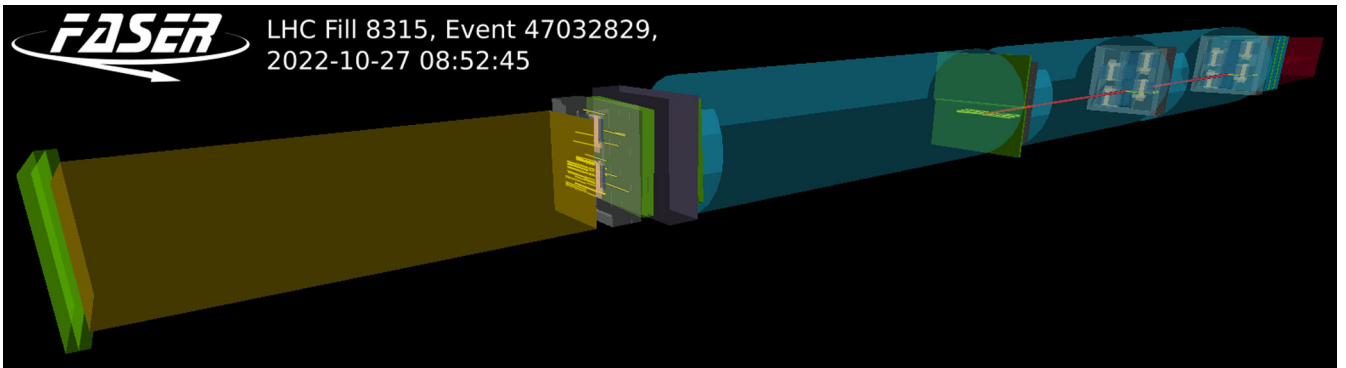


FIG. 6. Event display of a neutrino interaction candidate in which secondary particles produced in the CC interaction produce activity in the IFT.

TABLE II. The expected numbers of neutrino and anti-neutrino events from SIBYLL (first number) and DPMJET (second number) for an integrated luminosity of 35.4 fb^{-1} and different energy intervals, along with the sum over all energy intervals, and the average neutrino energy \bar{E}_ν . Results are shown requiring the interactions to be (i) in the FASER ν detector volume or (ii) in the target region and within a radius of 95 mm from the center of the FASER detector.

Volume	Type	$0 < E_\nu < 500 \text{ GeV}$	$500 < E_\nu < 1000 \text{ GeV}$	$E_\nu > 1000 \text{ GeV}$	Σ	$\bar{E}_\nu \text{ (GeV)}$
FASER ν	ν_μ	359/379	239/273	291/790	890/1442	880/1376
FASER ν	$\bar{\nu}_\mu$	116/130	62/85	49/151	227/367	657/1028
$r < 95 \text{ mm}$	ν_μ	147/154	105/118	141/375	394/647	943/1477
$r < 95 \text{ mm}$	$\bar{\nu}_\mu$	48/53	28/37	23/67	99/157	687/1057

case of perfect alignment of the FASER tracking detectors, we expect a momentum resolution of 2.1% at 100 GeV, 4.7% at 300 GeV, and 16.4% at 1 TeV. The accuracy of the alignment is validated using a photon conversion sample for momenta up to 250 GeV.

Appendix E: Expected number of neutrino events.—The predicted numbers of neutrino and antineutrino interactions from SIBYLL and DPMJET are listed in Table II. Results are shown requiring the interactions to be (i) in the FASER ν detector volume or (ii) in the target region and within a radius of 95 mm from the center of the FASER detector. Note that no additional acceptance and efficiency corrections are applied and the second requirement approximates the fiducial volume used in the analysis.

- [1] C. L. Cowan, F. Reines, F. B. Harrison, H. W. Kruse, and A. D. McGuire, Detection of the free neutrino: A Confirmation, *Science* **124**, 103 (1956).
- [2] G. Danby, J. M. Gaillard, K. A. Goulianos, L. M. Lederman, N. B. Mistry, M. Schwartz, and J. Steinberger, Observation of High-Energy Neutrino Reactions and the Existence of Two Kinds of Neutrinos, *Phys. Rev. Lett.* **9**, 36 (1962).
- [3] C. V. Achar *et al.*, Detection of muons produced by cosmic ray neutrinos deep underground, *Phys. Lett.* **18**, 196 (1965).
- [4] F. Reines, M. F. Crouch, T. L. Jenkins, W. R. Kropp, H. S. Gurr, G. R. Smith, J. P. F. Sellschop, and B. Meyer, Evidence for High-Energy Cosmic Ray Neutrino Interactions, *Phys. Rev. Lett.* **15**, 429 (1965).
- [5] Y. Fukuda *et al.* (Super-Kamiokande Collaboration), Evidence for Oscillation of Atmospheric Neutrinos, *Phys. Rev. Lett.* **81**, 1562 (1998).
- [6] R. Davis, Jr., D. S. Harmer, and K. C. Hoffman, Search for Neutrinos from the Sun, *Phys. Rev. Lett.* **20**, 1205 (1968).
- [7] B. T. Cleveland, T. Daily, R. Davis, Jr., J. R. Distel, K. Lande, C. K. Lee, P. S. Wildenhain, and J. Ullman, Measurement of the solar electron neutrino flux with the Homestake chlorine detector, *Astrophys. J.* **496**, 505 (1998).
- [8] T. Araki *et al.*, Experimental investigation of geologically produced antineutrinos with KamLAND, *Nature (London)* **436**, 499 (2005).
- [9] K. Hirata, T. Kajita, M. Koshiba, M. Nakahata, Y. Oyama *et al.* (Kamiokande-II Collaboration), Observation of a Neutrino Burst from the Supernova SN 1987a, *Phys. Rev. Lett.* **58**, 1490 (1987).
- [10] R. M. Bionta, G. Blewitt, C. B. Bratton, D. Casper, A. Ciocio *et al.*, Observation of a Neutrino Burst in Coincidence with Supernova SN 1987a in the Large Magellanic Cloud, *Phys. Rev. Lett.* **58**, 1494 (1987).
- [11] M. G. Aartsen *et al.* (IceCube Collaboration), Observation of High-Energy Astrophysical Neutrinos in Three Years of IceCube Data, *Phys. Rev. Lett.* **113**, 101101 (2014).
- [12] A. De Rujula and R. Ruckl, Neutrino and muon physics in the collider mode of future accelerators, in *Proceedings of the SSC Workshop: Superconducting Super Collider Fixed Target Physics* (1984), Vol. 5, pp. 571–596.
- [13] A. De Rujula, Neutrino physics at future colliders, in *Proceedings of the Trends in Physics, Prague 1984* (1984), Vol. 1, pp. 236–245.
- [14] F. Vannucci, Neutrino physics at LHC/SSC, Univ. Paris, Technical Report No. LPNHE-93-03, 1993, <https://cds.cern.ch/record/253670>.
- [15] A. De Rujula, E. Fernandez, and J. Gomez-Cadenas, Neutrino fluxes at future hadron colliders, *Nucl. Phys.* **B405**, 80 (1993).
- [16] H. Park, The estimation of neutrino fluxes produced by proton-proton collisions at $\sqrt{s} = 14 \text{ TeV}$ of the LHC, *J. High Energy Phys.* **10** (2011) 092.
- [17] J. L. Feng, I. Galon, F. Kling, and S. Trojanowski, ForwARD Search Experiment at the LHC, *Phys. Rev. D* **97**, 035001 (2018).
- [18] FASER Collaboration, Detecting and studying high-energy collider neutrinos with FASER at the LHC, *Eur. Phys. J. C* **80**, 61 (2020).
- [19] H. Abreu *et al.* (FASER Collaboration), First neutrino interaction candidates at the LHC, *Phys. Rev. D* **104**, L091101 (2021).
- [20] N. Beni *et al.*, Physics potential of an experiment using LHC neutrinos, *J. Phys. G* **46**, 115008 (2019).
- [21] C. Ahdida *et al.* (SHiP Collaboration), SND@LHC [arXiv:2002.08722](https://arxiv.org/abs/2002.08722).
- [22] G. Acampora *et al.* (SND@LHC Collaboration), SND@LHC: The scattering and neutrino detector at the LHC, [arXiv:2210.02784](https://arxiv.org/abs/2210.02784).
- [23] C. Ahdida *et al.* (SND@LHC Collaboration), Presentation ‘Results from SND@LHC’ at 57th Rencontres de Moriond presented by Ettore Zaffaroni, <https://indico.in2p3.fr/event/29681/contributions/122476/attachments/76427/110933/07-EZaffaroni-v1-public.pdf>.

- [24] J. L. Feng *et al.*, The Forward Physics Facility at the high-luminosity LHC, *J. Phys. G* **50**, 030501 (2023).
- [25] P. A. Zyla *et al.* (Particle Data Group), Review of particle physics, *Prog. Theor. Exp. Phys.* **2020**, 083C01 (2020).
- [26] M. Aartsen *et al.* (IceCube Collaboration), Measurement of the multi-TeV neutrino cross section with IceCube using Earth absorption, *Nature (London)* **551**, 596 (2017).
- [27] H. Abreu *et al.* (FASER Collaboration), The FASER Detector, [arXiv:2207.11427](https://arxiv.org/abs/2207.11427).
- [28] A. Ariga *et al.* (FASER Collaboration), Letter of intent for FASER: ForwArD Search ExpeRiment at the LHC, [arXiv:1811.10243](https://arxiv.org/abs/1811.10243).
- [29] A. Ariga *et al.* (FASER Collaboration), Technical proposal for FASER: ForwArD Search ExpeRiment at the LHC, [arXiv:1812.09139](https://arxiv.org/abs/1812.09139).
- [30] H. Abreu *et al.* (FASER Collaboration), The trigger and data acquisition system of the FASER experiment, *J. Instrum.* **16**, P12028 (2021).
- [31] J. Arakawa, J. L. Feng, A. Ismail, F. Kling, and M. Waterbury, Neutrino detection without neutrino detectors: Discovering collider neutrinos at FASER with electronic signals only, *Phys. Rev. D* **106**, 052011 (2022).
- [32] H. Abreu *et al.* (FASER Collaboration), The tracking detector of the FASER experiment, *Nucl. Instrum. Methods Phys. Res., Sect. A* **1034**, 166825 (2022).
- [33] A. Abdesselam *et al.*, The barrel modules of the ATLAS semiconductor tracker, *Nucl. Instrum. Methods Phys. Res., Sect. A* **568**, 642 (2006).
- [34] ATLAS Collaboration, Luminosity determination in pp collisions at $\sqrt{s} = 13$ TeV using the ATLAS detector at the LHC, [arXiv:2212.09379](https://arxiv.org/abs/2212.09379).
- [35] M. Aaboud *et al.* (ATLAS Collaboration), Luminosity determination in pp collisions at $\sqrt{s} = 8$ TeV using the ATLAS detector at the LHC, *Eur. Phys. J. C* **76**, 653 (2016).
- [36] C. Andreopoulos *et al.*, The GENIE Neutrino Monte Carlo Generator, *Nucl. Instrum. Methods Phys. Res., Sect. A* **614**, 87 (2010).
- [37] C. Andreopoulos, C. Barry, S. Dytman, H. Gallagher, T. Golan, R. Hatcher, G. Perdue, and J. Yarba, The GENIE Neutrino Monte Carlo generator: Physics and user manual, [arXiv:1510.05494](https://arxiv.org/abs/1510.05494).
- [38] F. Kling and L. J. Nevay, Forward neutrino fluxes at the LHC, *Phys. Rev. D* **104**, 113008 (2021).
- [39] S. Roesler, R. Engel, and J. Ranft, The Monte Carlo event generator DPMJET-III, in *Proceedings of the International Conference on Advanced Monte Carlo for Radiation Physics, Particle Transport Simulation and Applications (MC 2000)*, pp. 1033–1038.
- [40] A. Fedynitch, Cascade equations and hadronic interactions at very high energies. Ph.D. thesis, KIT, Karlsruhe, Dept. Phys., 2015, p. 11.
- [41] F. Riehn, R. Engel, A. Fedynitch, T. K. Gaisser, and T. Stanev, Hadronic interaction model Sibyll 2.3d and extensive air showers, *Phys. Rev. D* **102**, 063002 (2020).
- [42] S. Agostinelli *et al.* (GEANT4 Collaboration), GEANT4—a simulation toolkit, *Nucl. Instrum. Methods Phys. Res., Sect. A* **506**, 250 (2003).
- [43] A. Ferrari *et al.*, FLUKA: A multi-particle transport code (Program version 2005).
- [44] G. Battistoni *et al.*, Overview of the fluka code, *Ann. Nucl. Energy* **82**, 10 (2015). Joint International Conference on Supercomputing in Nuclear Applications and Monte Carlo 2013, SNA + MC 2013. Pluri- and Trans-disciplinarity, Towards New Modeling and Numerical Simulation Paradigms.
- [45] H. Dembinski and P. Ongmongkolkul *et al.*, [scikit-hep/iminuit, 10.5281/zenodo.3949207](https://arxiv.org/abs/10.5281/zenodo.3949207).
- [46] G. Cowan, K. Cranmer, E. Gross, and O. Vitells, Asymptotic formulae for likelihood-based tests of new physics, *Eur. Phys. J. C* **71**, 1554 (2011); **73**, 2501(E) (2013).
- [47] ATLAS Collaboration, The ATLAS Collaboration software and firmware, ATL-SOFT-PUB-2021-001, 2021, <https://cds.cern.ch/record/2767187>.
- [48] X. Ai *et al.*, A common tracking software project, *Comput. Softw. Big Sci.* **6**, 8 (2022).